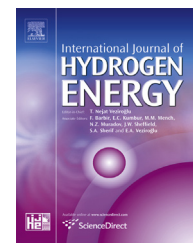


Available online at www.sciencedirect.com

ScienceDirect

journal homepage: www.elsevier.com/locate/hydro

Optimal power allocation for a FCHV based on linear programming and PID controller

Dima Fares^{a,*}, Riad Chedid^a, Sami Karaki^a, Rabih Jabr^a, Ferdinand Panik^b, Hugo Gabele^b, Ying Huang^b

^a Department of Electrical and Computer Engineering, American University of Beirut, P.O. Box 11-0236 Riad El Solh, Beirut 1107 2020, Lebanon

^b Mechanical Engineering Department, University of Applied Science, Esslingen, Germany

ARTICLE INFO

Article history:

Received 22 April 2014

Received in revised form

28 July 2014

Accepted 5 September 2014

Available online 11 October 2014

Keywords:

Fuel cell hybrid vehicles

Energy management system

Linear programming

Optimal control

ABSTRACT

Hybrid electric vehicles positively influence the transportation industry with regards to reducing the use of fossil fuels and minimizing polluting emissions. A class of such vehicles incorporates fuel cells and energy storage systems as alternatives to internal combustion engines. This paper develops a dynamically efficient energy management system for fuel cell hybrid vehicles for the purpose of achieving an optimal power allocation between the energy sources while adhering to component requirements and maintaining the essential operational performance. The paper addresses a two stage control methodologies, pre-driving optimization using linear programming algorithms and on-line optimization using PID controllers and component mechanisms. The performance criteria are based on the overall operational cost as well as the hydrogen consumption per trip. Comparison against a state control algorithm shows improvements in hydrogen consumption.

Copyright © 2014, Hydrogen Energy Publications, LLC. Published by Elsevier Ltd. All rights reserved.

Introduction

Environmental awareness regarding the dangers of polluting emissions and the drainage of energy resources has led to an extensive investment in research for alternative and clean energy resources. Regarding the transportation sector, trends are adopted in-order to develop new policies and trigger technological improvements in an attempt to surmount these effects. Fuel cell hybrid vehicle (FCHV) is one promising candidate, embedded with battery storage systems exhibit low emissions, high energy efficiency and independence on fossil fuel based resources.

The propulsion system of FCHV is equipped with fuel cells supplemented with a hydrogen tank and energy storage components. The addition of such power peaking sources results in further degree of freedom in the allocation of power resources. FC and battery systems aid each other to provide cruising power. The battery system is responsible to provide additional accelerating power as well as absorbing regenerative braking power.

Research is heading towards improving different components of the FCHV system such as the design of the FC [1,2], chemistry of the battery [3–5], hybridization topology [6], the technology and efficiency of the converters [7–9]. Moreover, they are indulged in the design and optimization of the energy

* Corresponding author. Tel.: +961 3 809859.

E-mail addresses: daf03@aub.edu.lb, dima.fares@gmail.com (D. Fares), rchedid@aub.edu.lb (R. Chedid), <http://dx.doi.org/10.1016/j.ijhydene.2014.09.020>

0360-3199/Copyright © 2014, Hydrogen Energy Publications, LLC. Published by Elsevier Ltd. All rights reserved.

Nomenclature			
LP	Linear Programming	I_{dc-in}, I_{dc-out}	DC/DC input and output currents, A
RB	State control Rule-based Method	I_{FC-req}	FC Current Request, A
PEM-FC	Proton exchange membrane fuel cells	I_{FCmax}	Maximum FC Current, A
NiMh	nickel–metal hydride battery	V_{bus}	Voltage at the DC Bus, V
SOC	State of Charge	P_{FC-req}	FC Power Request, kW
DOD	Depth of Discharge	I_{FC-net}	FC Net Current, A
n_{BT}	Number of battery cells	V_{FC}	FC Voltage, V
P_{FC}	FC output power, kW	\dot{n}_{H_2}	Hydrogen Consumption, /sec
P_{BT}	BT output power, kW	V_{BT-oc}	Battery open circuit voltage
P_{br}	Brake Power, kW	R_{BT}	Battery internal resistance
P_L	Load power, kW	T_{BT}	Battery temperature
P_{FCmin}, P_{FCmax}	FC minimum and maximum output power, kW	$I_{BT-ch-max}$	Battery maximum positively charging current
P_{BTmin}, P_{BTmax}	BT minimum and maximum output power, kW	$I_{BT-disch-max}$	Battery maximum negatively discharging current
SOC_{min}, SOC_{max}	Minimum and maximum SOC	α_{R-SOC}	Battery Resistance – SOC Factor
E_{BT}	Battery energy capacity, kWh	α_{R-T}	Battery Resistance – Temperature Factor
$R_{down-fc}$	FC Ramp down rate, kW	MH_o	Initial mass of H_2 molecules in the tank, grams
R_{up-fc}	FC Ramp up rate, kW	M_{H_2}	Molar Mass of Hydrogen, $kg\ mol^{-1}$
$R_{down-bt}$	BT Ramp down rate, kW	V	The volume of the fuel tank, m^3
R_{up-bt}	BT Ramp up rate, kW	T_{amb}	Ambient Temperature, $^{\circ}C$
γ_{FC}	Cost of H_2 consumption, $\$/kWh$	C_{H_2}	Cost of Hydrogen Fuel, $\$$
γ_{BT}	Cost of BT, $\$/kWh$	λ	Consumed rate of H_2 molecules per kW of energy
v	Vehicle speed, m/sec	Δt	Time duration
γ_{SL-FC}	Initial Cost of FC system, $\$/kWh$	N	Total number of time sample steps
H_{BT}	Battery heat capacity of battery, J/K	η_{BT}	Battery discharging efficiency
I_{BT}	Battery Current, A	GR	Gear Ratio
δ_{si-BT}	Entropy of cell reaction, J/(As K)	P_{m-min}	Minimum electric motor power, kW
β_{BT}	Battery damping factor	F_T	Total sum of forces, N
τ_{req}	Required Torque, Nm	F_w	Aerodynamic force, N
P_{motor}	Motor power, kW	F_r	Force of rolling resistance or friction losses, N
ω_m	Motor speed, rpm	F_i	Force due to inclination or load slope, N
P_{loss}	Motor power loss, kW	F_a	Acceleration force, N
S_{FC}	FC Status	ρ	Air density, $1.21\ kg/m^3$
C_r	Coefficient of rolling resistance, 0.014	A	Frontal area, $3.48\ m^2$
θ	Road inclination, degrees	v	Vehicle Speed, m/s
A	Vehicle acceleration, m/s^2	C_w	Air drag coefficient, 0.44
		m	Vehicle mass, kg
		g	Gravitational acceleration, $9.8\ m/s^2$

management system (EMS) [10,11]. Of importance is to find the best fit in scaling and managing the different power sources and storage units. The next section presents a detailed literature review of the different EMS studied for FCHV.

Optimum power allocation for FCHV

FCHV employ energy management systems to identify the power allocation among the different sources. The EMS addresses the power distribution among the different vehicle power sources in an attempt to meet the load demand while adhering to operational and component constraints. EMS algorithms range from simple rule based methods and heuristic approaches to complex optimization algorithms. The key element is the degree of knowledge of the driving cycle and the computational complexity of the algorithm [12]. There is a wealth of papers that addresses the design of the energy management systems in FCHV. A comprehensive review of

the state of art of FCHV architectures along with the most tackled approaches in EMS is presented in Refs. [13–15]. A comparative analysis between the different methods for the optimal power allocation is presented by Motapon et al [16]. EMS is tested for different driving scenarios such as highway driving cycle, urban driving cycle, fast acceleration and maximum driving distance [17]. In addition, EMS is designed to satisfy the five different modes of operation in FCHV which are starting, cruising, passing, braking and stopping.

Two kinds of EMS controllers are addressed, off-line controllers and on-line controllers [18]. Off-line controllers use intelligent or non-intelligent approaches in order to find the optimal power split between energy sources in an attempt to minimize hydrogen fuel consumption or system cost. Optimization approaches can use linear programming techniques [19], dynamic programming [20], stochastic dynamic programming [17], game theory [21], genetic algorithm [22], load shifting [23], equivalent consumption minimization strategy,

control theory [24,25], neural networks [26–28], predictive controllers [29,30], adaptive optimal control [31], thermostat and power follower controls [32,33] and H-infinity control [34].

On-line controllers are real time controllers, which use PI controllers, frequency decoupling strategies or rule based controllers. Rule based EMS excels in real time applications because it does not require prior knowledge of the driving cycle. However, it is based on heuristics and expertise of the EMS designer. It is easy, simple and based on engineering intuition. Rule based methods can be either fuzzy or deterministic approaches such as state machine control. State machine control is based on persons expertise as well as heuristic approaches [35–37]. The performance of such a method is highly dependent on the approach and the efficiency of the rules. The main drawback is the hysteresis component that results from the switching between the states. Deterministic rule based EMS are usually based on look-up tables where demand actions are known [38].

Tate et al. used linear programming [19] techniques to optimize the split of power between an internal combustion engine (ICE) and a battery system. The method is formulated as a convex problem and then approximated as a large linear program. To account for the change in battery efficiencies during charging and discharging, they implemented them as two separate variables. On the other hand, the whole power train is modeled on efficiency basis. In Ref. [39], we adopted the same methodology to a FCHV and implemented a controller based on linear programming technique, however we did not test the results on the vehicle model so it was just an off-line power allocation of the sources. The main issue with linear programming is that it can give us a gist of the control while mainly to model the components in the FCHV powertrain high levels of non-linearity is involved.

This paper tackles contemporary issues in the energy management system of the FCHV. It addresses a two stage control methodologies, pre-driving optimization algorithms and on-line optimization using PID controllers. In the first stage, linear programming is used to achieve the global optimum of a known driving cycle. System losses are considered in order to achieve a fair approximation of system components. Linearization of cost and hydrogen consumption functions aid in the use of linear programming. During on-line optimization which is done using a complete Simulink designed model of the fuel cell hybrid vehicle, linear programming techniques are used to test the efficiency of such algorithms in lowering operational cost while ensuring drivability. PID controllers minimize the error between the actual and approximated vehicle speeds.

The performance criteria are based on the overall operational cost as well as the hydrogen consumption per trip. Moreover, battery state of charge and system efficiencies are also measured and analyzed. The methodology yields several outcomes in lowering system cost, improving efficiency of the drive train and prolonged life of FC and battery. Comparison with a state space EMS will highlight the distinct features of the methodology. Comparison is done between a controller using the optimization algorithms for the whole driving cycle and a controller using state machine rule based techniques. Results indicate a reduction in system cost and in hydrogen fuel consumption. Moreover, the results highlight the

importance of using optimizing algorithmic in urban driving cycles since reduction in hydrogen consumption is much higher compared to highway cycles.

System description

The construction of the FCHV subsystem models is performed using a graphical simulation environment software (MatLab/Simulink). It is essential for the models to emulate the real dynamics of the vehicle in-order to have efficient simulation results. The FCHV is composed of at least ten different subsystems. The sources in the subsystem are a primary one-way energy source unit and a secondary bi-directional storage component. The former source is a PEM fuel cell system and the latter is a NiMH battery. The mathematical models that govern these subsystems encompass high levels of computational complexity. For this reason, simple dynamic equations as well as test-benched experimental results indexed as lookup tables are used to model the subsystems in Simulink. This Simulink model, is a feed forward backward model of the subsystems based on a distributed control system with a CAN bus communication method. The CAN network is designed to regulate the performance of the FCHV. An energy management system strategy based on linear programming optimization algorithms is formulated to coordinate the power split between the sources.

The vehicle considered is a light duty sprinter with a parallel drive train embedding a 70 kW induction electric motor, a 70 kW FC System and a 1.9 kWh battery system. The selection of the sizes is based on the Mercedes-Benz Sprinter used for the EU project HySYS (FP6) [40]. However, a 70 kW FC is used for research instead of the 80 kW FC used in the EU project. The system topology is shown in Fig. 1. The FC is connected to the DC bus via a DC/DC converter that serves to stabilize the voltage at the bus. The battery system is joined to the DC bus in parallel using a bi-directional DC/DC converter. This enables the battery to discharge current into the system to serve

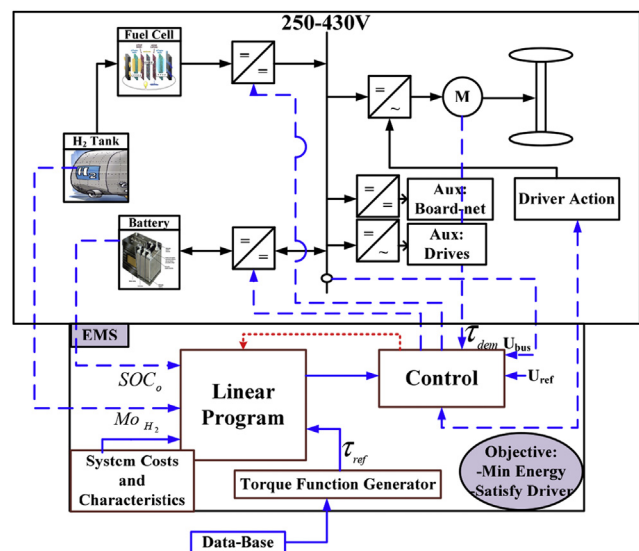


Fig. 1 – System topology.

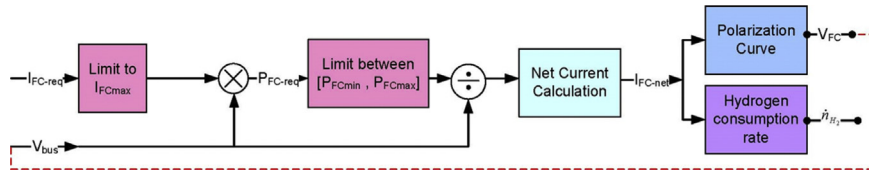


Fig. 2 – FC Simulink model.

the load, and charge current during regenerative braking. The electric motor is connected to the DC bus via a DC/AC inverter. It is serially coupled to the transmission system and wheels. Vehicle auxiliaries are connected to the DC bus using two branches. The first branch connects the 24V DC board to the bus using a DC/DC converter. The other branch embeds a DC/AC inverter to join the DC bus to the electric drives of the subcomponents such as the air conditioning, servo brakes and water pumps. During offline optimization the linear program block considers the initial battery SOC and the available hydrogen in the tank. As inputs to the program are the system costs and vector of fixed input values which are $(\gamma_{FC}, \gamma_{SL-FC}, \gamma_{BT}, E_{BT}, P_{FC-min}, P_{FC-max}, P_{BT-min}, P_{BT-max}, SOC_{min}, SOC_{max}, R_{down-fc}, R_{up-fc}, R_{down-bt}, R_{up-bt}, \lambda, MH_0)$.

Fuel cell system model

Fuel cell systems are composed of cells that convert the chemical energy present in hydrogen fuel into electrical energy by oxidation–reduction reaction. They produce a continuous amount of electricity as long as it is provided with fuel and oxygen to maintain the reaction process. Proton exchange membrane fuel cells (PEM FC), are usually used in vehicular applications due to their fast start-up time, high power density and low operating temperature [10]. Their transient performance when responding to load demand is limited due to the chemical reactions that occur in the FC.

To build a fast and correct Simulink model of the FC, lookup tables are used to approximate its performance. These

tables were derived from experimental testing on an actual FC test-bench in the labs of the University of Applied Sciences of Esslingen Germany. Fig. 2, shows a schematic of the FC system adopted in the Simulink model. The current requested from the FC (I_{FC-req}) is limited to the maximum current (I_{FCmax}) that could be supplied by the FC according to the manufacturer's data sheet. Then the power required from the FC is calculated by multiplying the requested current with the corresponding voltage of the DC bus (V_{bus}). The FC power request (P_{FC-req}) is also limited between the maximum (P_{FCmax}) and minimum (P_{FCmin}) power of the FC that are provided in the data sheet. From the resulting FC current request, the net current request is computed using the net current curve in Fig. 3 which considers the fuel cell efficiency. Then, the net current is used to calculate the FC voltage using the polarization curve in Fig. 4. The latter takes into consideration the losses in the FC system such as activation and ohmic losses. Finally, using the net FC current request, the hydrogen consumption is approximated using the hydrogen consumption curve in Fig. 5. This curve is a function of the current requested from the FC. In this paper, the characteristics of the chosen FC is shown in Table 1.

Battery system

The next building block of the FCHV power-train is the NiMH battery system. The battery characteristics are shown in Table 2. The optimum range of the battery SOC is derived using a test benched process and is found to be located between 0.55 till 0.65.

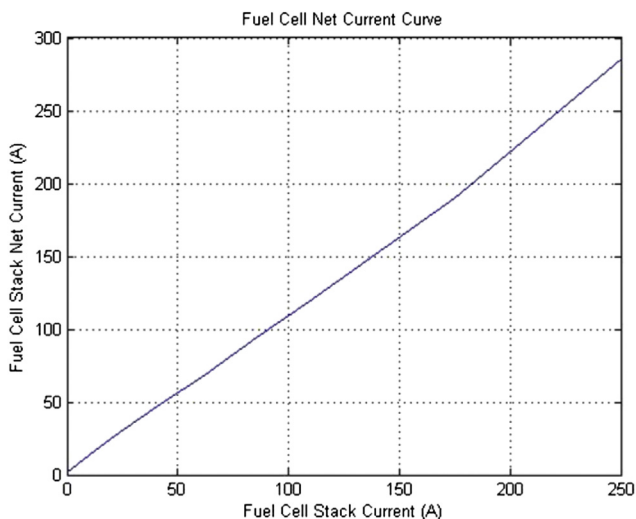


Fig. 3 – FC net current curve.

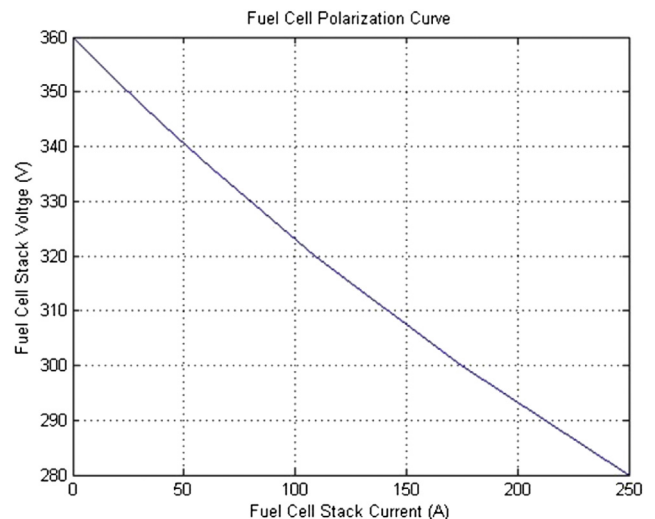


Fig. 4 – FC polarization curve.

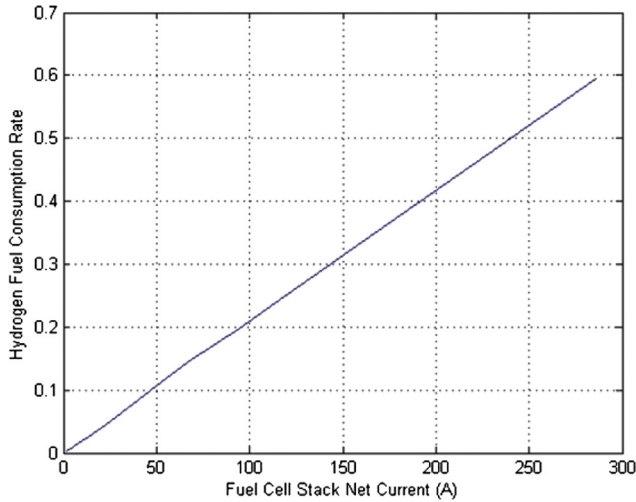


Fig. 5 – Hydrogen fuel consumption rate.

In Simulink, the battery controller is used to monitor and calculate the maximum charging and discharging currents that are permissible. The battery control system calculates the maximum charge and discharge limits of the battery system depending on the SOC level, open circuit voltage (V_{BT-oc}), internal resistance (R_{BT}) and temperature (T_{BT}). The maximum positively charging current is shown in equation (1) and the maximum negatively discharging current is shown in equation (2).

$$I_{BT-ch-max} = \begin{cases} \frac{V_{BT-max} - V_{BT-oc}}{R_{BT}} & SOC < SOC_{max} \\ 0 & SOC \geq SOC_{max} \end{cases} \quad (1)$$

$$I_{BT-disch-max} = \begin{cases} \frac{V_{BT-min} - V_{BT-oc}}{R_{BT}} & SOC > SOC_{min} \\ 0 & SOC \leq SOC_{min} \end{cases} \quad (2)$$

The Simulink model for the battery is shown in Fig. 6. It receives the battery current request and accordingly computes the battery voltage depending on the SOC, internal resistance and temperature. It is composed of four different blocks that are interconnected. In the SOC generation block, the SOC is updated from the current value inputted to the block by current integration. The battery modeled that is adopted for this paper has certain characteristic factors shown in Table 2.

Table 1 – Fuel cell characteristic table.

FC Current ramp up/down rates (A/s)	[290, 290]
FC Power ramp up/down rates (kW/s)	[5, -5]
FC max. power (kW)	70
Resistance factor for series and parallel connection	40
FC stack number of cells	350
FC OCV (V)	345.8
FC minimum voltage (V)	250
FC maximum voltage (V)	430
Area for heat exchange on stack surface (m ²)	1.5

Table 2 – Battery system characteristic table.

Number of cells in series	80
Number of cells in parallel	1
Nominal capacity of battery [Ah]	6.5
Minimum/maximum BT voltage [V]	160/328
Nominal battery voltage [V]	288
Temperature coeff. for OCV [V/K]	-0.000134161
SOC at simulation start	0.8
Battery ambient temperature [°C]	20
Battery voltage at start of simulation [V]	280.75
Battery resistance at start of simulation [ohms]	0.3186
Max. charge/Disch. I [A] at 25 °C, 60% SOC	155/-360
Max. charge/Disch. P [kW] at 25 °C, 60% SOC	50.8/-57.5
Battery volume estimation [m ³]	0.012
Maximal battery temperature [°C]	50
Module weight [kg]	1.02
Power density [W/kg]	137.6471

The open circuit voltage generation block adds the effect of SOC and temperature according to equation (3). The open circuit voltage depends on the current SOC level so $V_{BT-oc}(SOC)$ is estimated according to Fig. 7. Then the battery voltage can be derived accordingly depending on the ambient temperature and the actual battery temperature. Note that at the beginning of the simulation the battery temperature is equal to the ambient temperature.

The battery internal resistance R_{BT} for a level of SOC and for a specific battery temperature is calculated using the method in equations (4) and (5). Figs. 8 and 9, indicate the resistive factor added to the battery during charging and discharging processes depending on the SOC level as shown also in equation (4). Similarly, Fig. 10 shows the relation between resistance and battery temperature as shown also in equation (4). Therefore, after interpolating the factors α_{R-SOC} and α_{R-T} using Figs. 8–10 respectively, the battery internal resistance can be computed using equation (5).

To calculate the temperature changes in the battery in degrees Celsius, a simple equation is adopted based on the thermodynamics system inside the battery. It is the

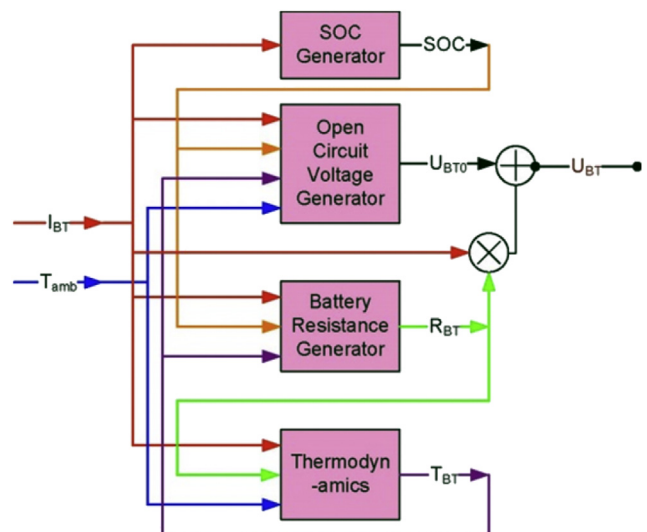


Fig. 6 – Battery Simulink model block diagram.

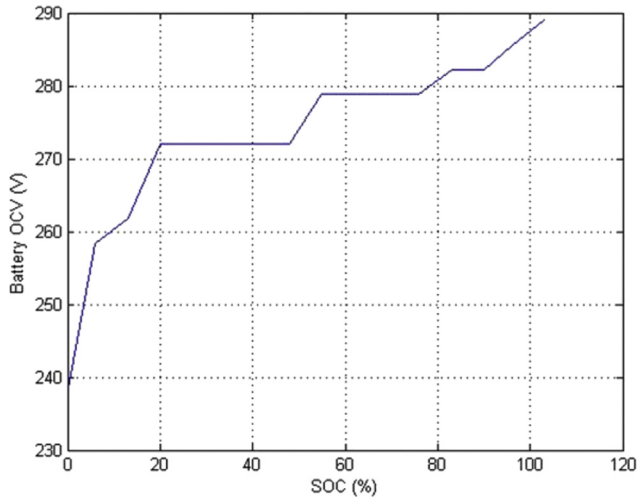


Fig. 7 – OCV dependence on SOC.

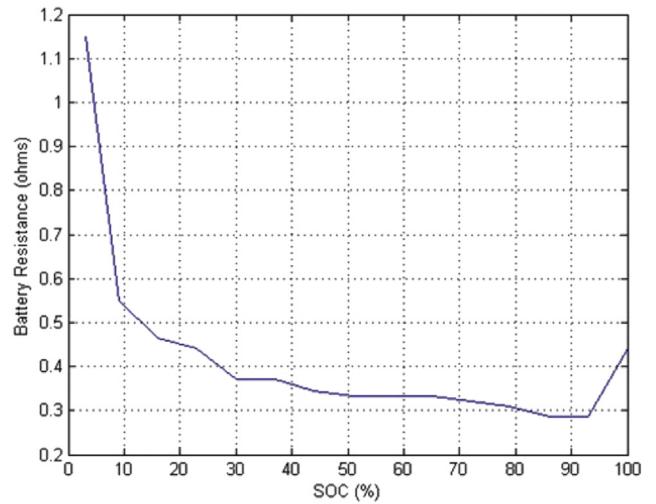


Fig. 9 – Resistance dependence on SOC during discharging.

continuous integration of three factors as shown in equation (6). The first factor is the heat loss by the current; the second is the entropy generator which multiplies the battery current and number of cells and temperature in kelvin by entropy of cell reaction factor. Finally, the third factor is the difference between the ambient and battery temperature multiplied by the battery thermal resistance which depends on power in each cell with respect to area. Finally, the output voltage of the battery system is calculated in equation (7).

$$V_{BT-oc} = \beta_{BT} V_{BT-oc0}(SOC) + (\alpha_{OCV}[T_{BT} - T_{amb}]n_{BT}) \quad (3)$$

$$\alpha_{R-SOC} = f(SOC) \quad \alpha_{R-T} = f(T_{BT}) \quad (4)$$

$$R_{BT} = \alpha_{R-SOC} \alpha_{R-T} \quad (5)$$

$$T_{BT} = \int \frac{1}{H_{BT}} [I_{BT}^2 R_{BT} + n_{BT} I_{BT} \delta_{si-BT} (T_{BT} - 273) + 32(T_{amb} - T_{BT})] \quad (6)$$

$$V_{BT} = V_{BT-oc} + R_{BT} I_{BT} \quad (7)$$

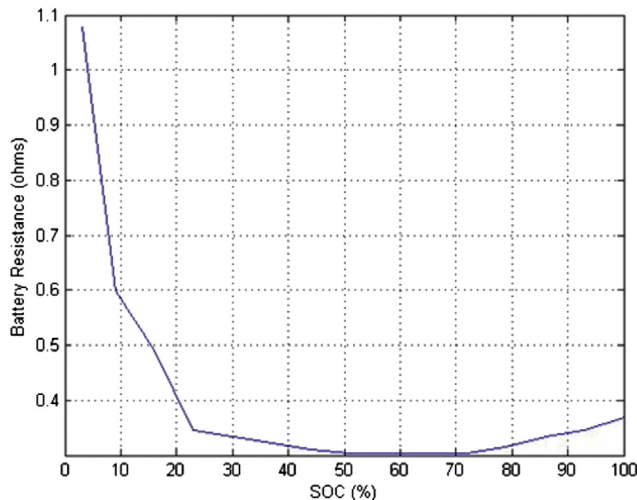


Fig. 8 – Resistance dependence on SOC during charging.

Drivers model subsystem

The driving cycle is usually indexed by a velocity profile. The user can choose between the common known cycles such as FTP-75, FUDS, Highway, JAP-1015, NEFZ or can generate a user defined cycle. The driver's model subsystem is responsible to send control signals to the energy management system. These signals represent the magnitude of the accelerating and braking torques. The derivation of these signals is based on the reference speed set by the user and the actual vehicle speed measured at the level of the wheels. In order to minimize the speed difference between the referenced value and measured value, a proportional integral derivative controller (PID) is adopted. This type of controllers is widely used in the control systems in-order to minimize the error between the measured and the desired process value.

The PID controller consists of three parallel blocks: Proportional, Integral and Derivative. The proportional part reduces the most of the overall error while the integral part drives the system to a smaller error. Finally, the derivative

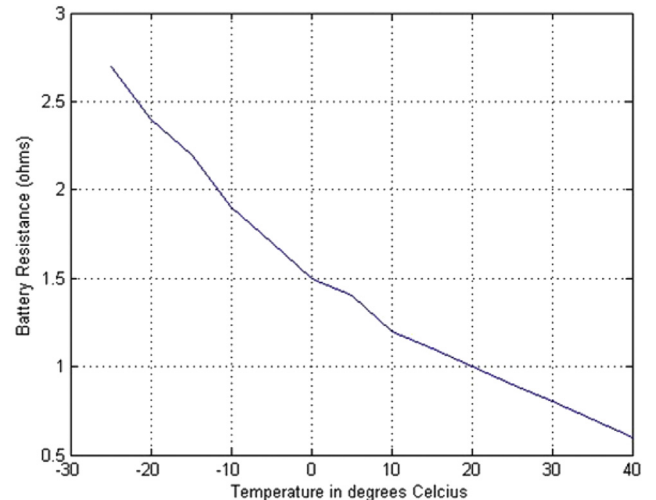


Fig. 10 – Resistance dependence on temperature.

Table 3 – Drivers model characteristic table.

Controller proportional factor K_p	130
Controller integral factor K_i	2
Controller derivate factor K_d	1
Avoid integrator overflow factor a_w	0.05

part minimizes the overshoot and reduces settling time of the overall system. Equation (8) calculates the torque demand. This torque is limited to the maximum torque of the vehicle electric motor which is 230Nm in this case. The error factor $e(t)$ is the difference between the measured speed and the reference speed. Table 3, indicates the values of the parameters of the PID controller. These values resulted from testing and tuning the controller to fit the Simulink model.

$$\tau_{req}(t) = K_p e(t) + K_i \int e(t) dt + K_d \frac{d(e(t))}{dt} \quad (8)$$

Vehicle model subsystem

The total sum of forces (F_T) acting on the wheels are the aerodynamic force (F_w), the force of rolling resistance or friction losses (F_r), the force due to inclination or load slope (F_i) and the acceleration force (F_a). These forces are described by equations 9–12. The power demanded by the vehicle as a function of speed is given in equation (14). For simplicity, the road is considered to be flat and therefore θ is zero.

$$F_w = (1/2)\rho A_f C_w v^2 \quad (9)$$

$$F_r = mg C_r \cos(\theta) \quad (10)$$

$$F_i = mg \sin(\theta) \quad (11)$$

$$F_a = ma \quad (12)$$

$$F_T = F_w + F_r + F_i + F_a \quad (13)$$

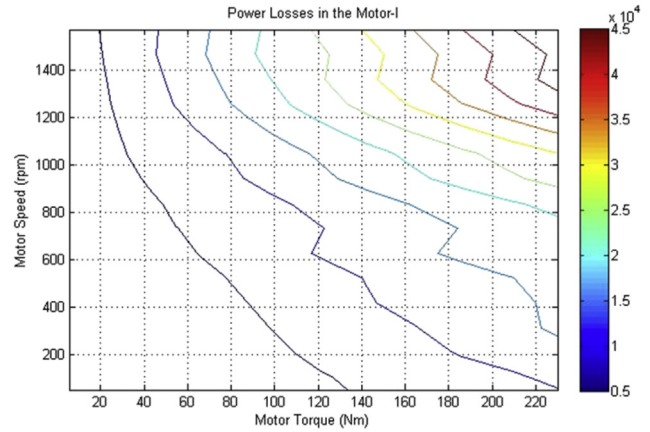
$$P_w = v F_T \quad (14)$$

Electric motor subsystem

In FCHV, there is one propulsion driving source which is the electric motor. Its size is determined at early stage of power train design to satisfy the peak power requirements [17]. Models of the electric motors have a high degree of complexity especially if one tried to incorporate them into a bigger model.

Table 4 – Electric motor characteristic table.

Continuous power (kW)	70
Peak power (kW)	90
Continuous torque (Nm)	180
Peak torque (Nm)	230
Max speed (rad/s)	1248.8
Motor mass (kg)	50
C_p (J/kg K)	1500
Surface area (m ²)	0.5
Heat transfer coeff. (W/m ² K)	10
Motor Inertia (kgm ²)	0.1098

**Fig. 11 – Power losses in the motor and inverter system.**

Failure to provide a fast response time can crash the whole model. For this reason, in FCHV control applications, the electric motor is modeled as a static entity with certain power losses [41]. The power losses and efficiency maps are usually referred to by look-up tables.

The electric motor Simulink block translates the power demanded from the sources to torque and speed to drive the wheels. Table 4, indicates the motor characteristics. The losses in the motor and inverter are handled using 2-D lookup table based on the rotor speed and output torque. The dynamics of the electric motor are ignored because the period of the power train of the FCHV is much larger than the period of the motor dynamics. This is why it is redundant to go into the motor dynamics. Therefore, the motor is modeled with its efficiency maps as shown in Fig. 11 and equation (15).

$$P_{motor} = f(\tau_{req}, \omega_m) = \tau_{req} \omega_m + P_{loss} \quad (15)$$

Transmission subsystem

The transmission system translates the torque from the motor system into gear ratio, torque and speed values to the wheels. The gear box is based on the motor speed and thus alters the gearshift lever consequently. After the gear command is generated, it is translated to a gear ratio. In FC the gear is always at one and so the gear ratio is 13.

Auxiliaries subsystem

The Simulink model considers the auxiliary power that is required from the FCHV components. These include the power required from the cooling system, power braking (20 W), power steering (120 W), air-conditioning (600 W) and fuel-cell system auxiliaries (1000 W).

Power conditioning subsystem

The power conditioning of the FCHV is composed of two components. The first is a DC/DC two-way converter connected between the battery and the DC bus. The second is the inverter which transforms the DC power from the bus into AC

current to be fed to the electric motor. The latter is modeled as power losses along with the electric motor losses.

The DC/DC converter allows the passage of current from DC bus to the battery system and vice versa depending on the voltage level on both sides. The current at the input of the converter I_{dc-in} is related to the current at the output I_{dc-out} of the converter. Table 5 indicates the characteristic data of the DC/DC converter adopted for this paper.

Energy management system block

The main subsystem in the FCHV is the energy management system (EMS) block. The EMS block, is the main drive of the FCHV since it organizes the power allocation between the FC system and the battery system. The algorithms that are dealt with in this paper exhibit a slow response time especially when compared to the response time of the FCHV. For this reason, the EMS is tweaked for it to be adaptable to all algorithmic scenarios. This is accomplished by using lookup tables linked directly to the output of the algorithmic blocks in the Matlab files environment.

The FC status block pinpoints the conditions in which the FC is turned off S_{FC} . There are four lookup tables embedded in the EMS block. These lookup tables are derived beforehand from the algorithmic techniques discussed in the forthcoming chapters. All tables are horizontally indexed by the cycle time of the FCHV. Vertically, they are indexed by the FC power requirements, battery power requirements, motor torque request and braking torque request. Fig. 12, reveals a topologically view of the above mentioned design. The FCHV model is based on current calculations and not power computations. For this reason the FC and battery power requests are translated into current request by dividing those requests with the voltage at the DC bus.

Problem formulation

The problem formulation is a constrained optimization problem with linear constraints. The main aim is to find the optimal power allocation between the components of the FCHV, thus to find the power required from the FC (P_{FC}) and the power required from the battery (P_{BT}). The cost function is depicted in equation (16).

$$\min \left[\sum_{t=1}^N [(\gamma_{FC} + \gamma_{SL-FC})P_{FC}(t) + (\gamma_{BT})P_{BT}(t) + \gamma_{FC}P_{br}(t)]\Delta t \right] \quad (16)$$

The cost minimization function considers four factors.

Table 5 – Power conditioning characteristic table.

Current Limit in buck mode during battery charging (A)	40
Current Limit in boost mode during battery discharging (A)	–40
Buck converter efficiency	0.96
Boost converter efficiency	0.96
Converter specific weight (kW/kg)	2

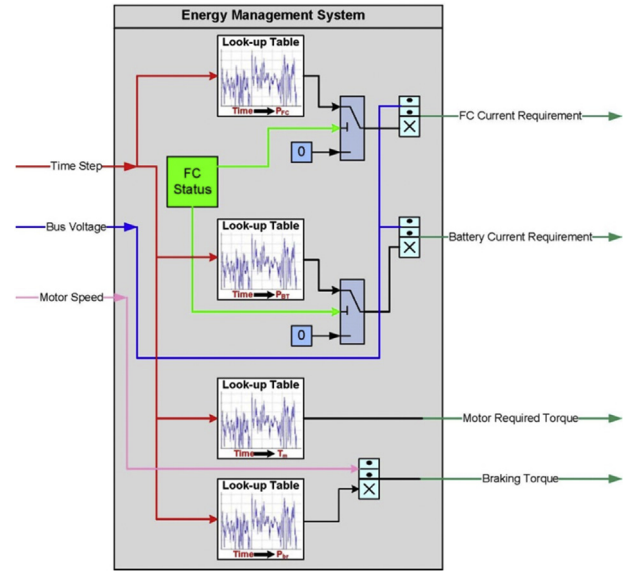


Fig. 12 – EMS topological model.

First the cost of hydrogen consumption, then the cost of operating the FC as it consumes power. The third factor is the cost of discharging the battery power. Finally, the cost of power dissipation which occurs when the battery is fully charged and the load is generative. Thus the cost function considers the life cycle of the FC.

System constraints

The system constraints are the following:

$$SOC(t) = SOC(t-1) - (P_{BT}(t)\Delta t)/(\eta_{BT}E_{BT}) \quad (17)$$

$$P_{FC}(t) + P_{BT}(t) - P_{br}(t) = P_L(t) \quad (18)$$

$$P_{FCmin} \leq P_{FC}(t) \leq P_{FCmax} \quad (19)$$

$$P_{BTmin} \leq P_{BT}(t) \leq P_{BTmax} \quad (20)$$

$$SOC_{BT-min} \leq SOC(t) \leq SOC_{BT-max} \quad (21)$$

$$R_{down-fc}\Delta t \leq P_{FC}(t) - P_{FC}(t-1) \leq R_{up-fc}\Delta t \quad (22)$$

$$R_{down-bt}\Delta t \leq P_{BT}(t) - P_{BT}(t-1) \leq R_{up-bt}\Delta t \quad (23)$$

$$\sum_{k=1}^N \lambda P_{FC}(t)d(t) \leq MH_o \quad (24)$$

The SOC period coupling constraint shown in equation (17), computes the SOC of the battery at each instance in time depending on the current battery power and previous SOC. The deducted charge represents the fraction of energy from the total energy available in the battery spent at time t . The power balance constraint in equation (18) ensures the load is always supplied with the needed amount of energy whether from battery or FC. The system discards the extra power via P_{br} , which is usually the case when the battery is fully charged

and the load demand is generative. Constraints shown in equation (19), equation (20) and equation (21) are limitation constraints for the supplied power of the FCHV components. The ramp rate constraints in equation (22) and equation (23) limit the ramp rate of both the FC and the battery. These are essential to prevent oxygen starvation of the FC system which occurs when a high instantaneous power is required from the FC. The storage capacity constraint shown in equation (24) guarantees that the hydrogen tank is able to cover the whole trip.

The cost of the battery and fuel cell system that are shown in the LP formulation can be assumed from the research. For the FC, the current cost is approximately 5000\$/kW for 5000 h under cycling conditions [42]. Therefore, the service life of the FC can be approximated to 1\$/kWh. The rate of consumption of hydrogen molecules per kW is averaged from the Simulink model at about 0.01 g/kWs. The cost of hydrogen is approximated to be 3\$/kg which makes the kW cost of hydrogen consumption equal to 0.161 \$/kWh. According to the annual energy outlook report, the cost of the battery for electric vehicle in 2014 is approximately 700 \$/kWh [43]. NiMH batteries for vehicular applications have a lifetime of more than 1000 cycles [44]. By choosing the battery cycle lifetime of 1000 cycles, it can be speculated that the battery service life is around 0.7 \$/kWh which is 70% of the FC service life.

Finally, the initial mass of hydrogen molecules available in the tank is calculated by using the ideal gas equation. The tank has a volume of 0.08 cubic meters and is maintained at a pressure of 300 atm. Therefore, after calculating the number of moles (n), the initial molar mass of hydrogen in the tank is estimated to be 1970g.

Simulation results

The linear programming algorithm along with the PID controller methodology discussed in the previous sections is applied, tested and analyzed for known driving cycles. A multiple of simulated comparative experiments demonstrates the efficiency, significance and applicability of the algorithmic strategy. It is tested for known driving cycles such as highway and the FUDS driving cycles. The outcome of the algorithm is the optimal power split between the FC and the battery. This is injected in the vehicle Simulink model which incorporates also PID controllers. The behavior of the system resources and electric motor is analyzed and the hydrogen consumption is compared against the state machine controlled. The vehicle component parameter used for simulation is shown in Table 6.

Table 6 – Vehicle component parameters.

FC power limits (kW)	[0 70]
BT power limits (kW)	[-40 40]
SOC limits	[0.5 0.9]
Initial SOC	0.8
Final SOC	0.8
FC ramp rates (kW/s)	[-10 5]
BT ramp rates (kW/s)	[-15 8]

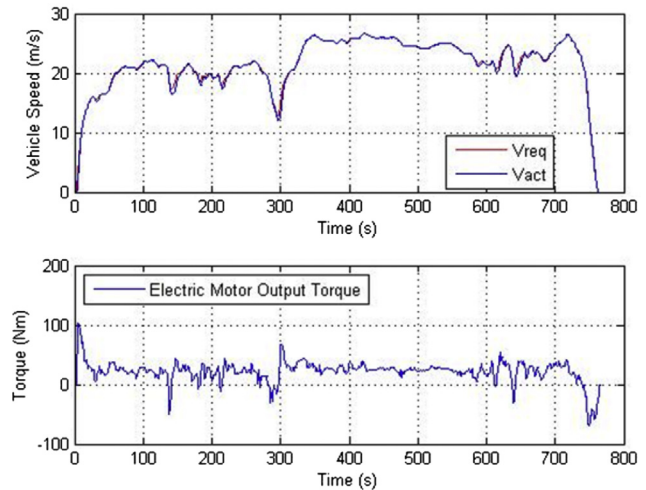


Fig. 13 – Speed and torque curve for highway driving cycle.

Highway driving cycle

The highway driving cycle is characterized by slow dynamics and high speed points. Fig. 13 shows the vehicle speed from the Simulink model. There are two speeds in the upper window of the figure, the actual vehicle speed (V_{act}) and the required vehicle speed (V_{req}). The former speed is calculated in the Simulink model based on the actual forces acting on the vehicle and the total moment of inertia of the vehicle. The required vehicle speed is specified by the user for the respective driving cycle. These two speeds are approximately overlapping by the help of the PID controller that tried to minimize the error between the actual and required speed. The second part of the figure dictates the electric motor output torque required. Fig. 14 reveals the power allocation in-order to meet the load demand. The battery is usually charging when the load is generative and FC is the main source supplying the load. The 1.9 kWh battery aids the 70 kW FC when needed. After 450 s the battery stopped discharging so as to maintain the required final SOC. A snapshot of the power allocation is shown in Fig. 15 where the battery is shown to contribute to the load much less that the FC due to its

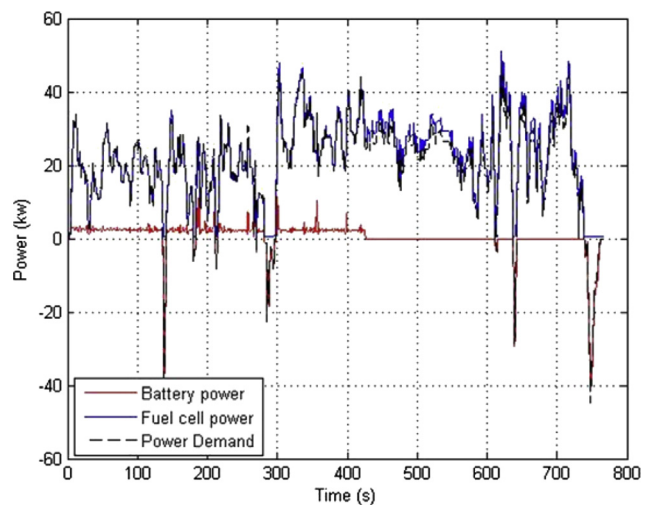


Fig. 14 – Power sources for highway driving cycle.

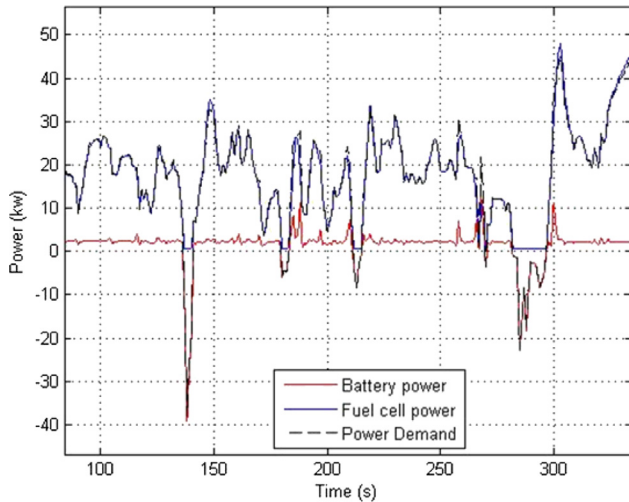


Fig. 15 – Episode of the power sources for highway driving cycle.

size. Fig. 16 shows the FC currents, it is clear that the net current is greater than the current request almost all the time due to the losses adding up in the FC. However, at instances when the FC net current is less than the FC current specifically around 300s, a dip in the actual speed is also witnessed. So the system is trying to readjust its variables. A snapshot of this incident is shown in Fig. 17. Fig. 18 shows the behavior of the battery SOC during the cycle and how it maintains its starting SOC. Finally, Fig. 19 reveals a snapshot of the DC bus voltage and indicates that it is maintained between 305 and 360V. The data of the results is shown in Table 7. It is revealed that the FC is the main source in supplying the demand. The cost of operation which includes the life cycle costs of the system components is \$4.6.

FUDS driving cycle

FUDS is characterized by fast dynamics since it is close to an urban cycle. The characteristic speed curves resulting from the PID controllers of the Simulink model is shown in Fig. 20. Also the electric motor output torque is revealed. The power

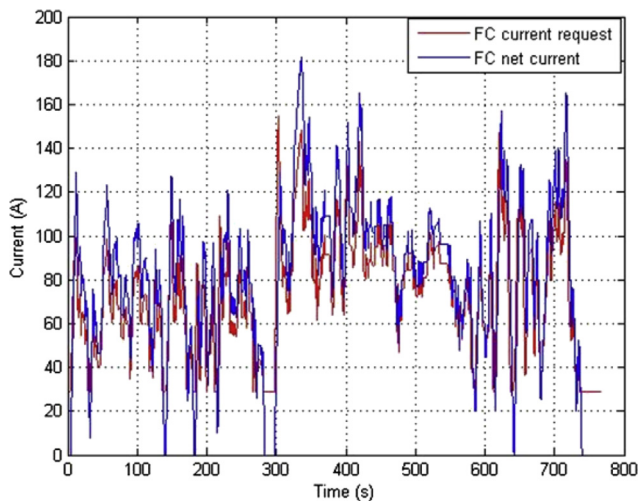


Fig. 16 – Fuel cell currents for highway driving cycle.

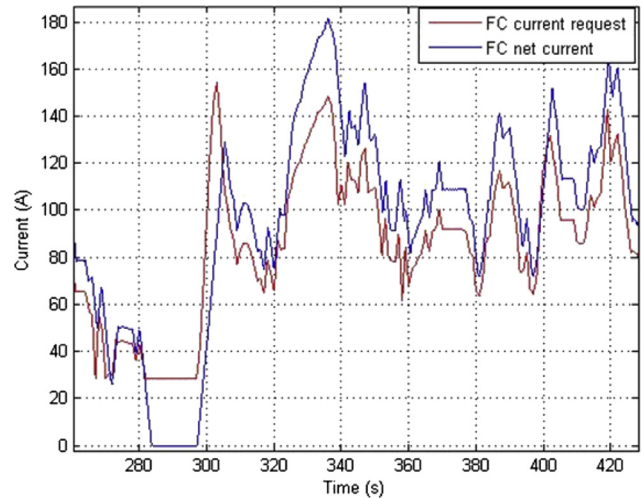


Fig. 17 – Episode of fuel cell currents for highway driving cycle.

allocation in Fig. 21 directly grabs to the attention that the battery is exploited more using this driving cycle. This is due to the frequent decelerations that lead to regenerative braking energy and thus battery charges. This is revealed in Fig. 22. Fig. 23 shows at different instances that the battery and FC are working together in order to supply the load. The net and required currents from the FC are shown in Figs. 24 and 25, however unlike the highway cycle; the net current is always greater than the required current. It is also witnessed that during this cycle the speed dips are not that visible. This is because the cycle does not have high speeds. Fig. 26 shows the behavior of the battery SOC throughout the cycle. Finally, the DC bus voltage is maintained within 305 and 360V as shown in Fig. 27. Table 8 dictates the numerical results with a cost of \$2.2.

Effect of increasing the battery capacity

The effect of increasing the battery capacity is also considered. It is known as a rule of thumb that by increasing the battery capacity, the mass of the battery will increase and thus

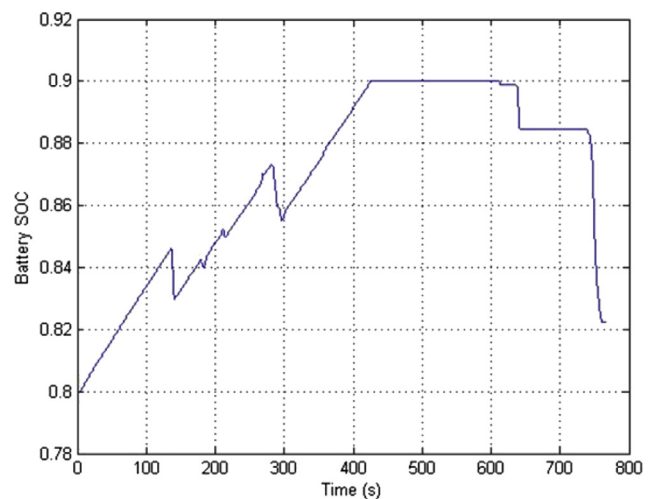


Fig. 18 – SOC for highway driving cycle.

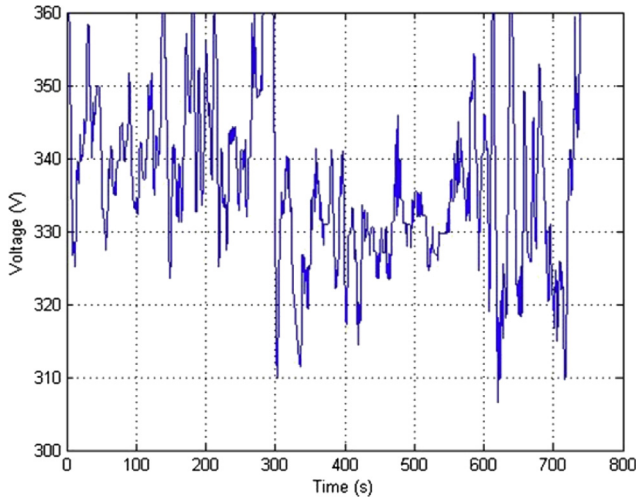


Fig. 19 – DC bus voltage for highway driving cycle.

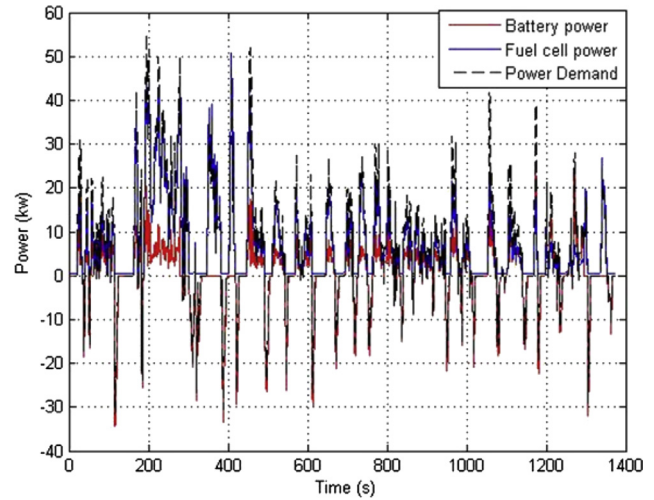


Fig. 21 – Power sources for FUDS driving cycle.

Table 7 – LP results for highway driving cycle.

Electric energy demand (kWh)	4.23
Electric energy supplied by FC (kWh)	3.97
Electric energy supplied by BT (kWh)	0.36
Electric energy dissipated through brake (kWh)	0.004
Final state of charge of BT	0.6
Cost of operation (\$)	4.6

the weight of the vehicle will increase. This will affect the forces acting on the vehicle and will therefore increase the total demanded load. For this reason, the battery capacity is usually bounded. However, it will be assumed that when the battery capacity increases by 1 kWh then the size will increase by 10 kg. By doubling the 1.9 kWh battery to 3.8 kWh, the vehicle mass will increase by 20 kg. Table 9 indicates the results of such an increase for both driving cycles considered. It is noted in both driving cycles that by increasing the battery size, lower hydrogen consumption and thus lower operational cost are achieved. Urban driving cycles use the battery more

than highway driving cycles. This is due to the increased use of brake through stopping and starting in urban cycles. Thus a 23% cost reduction is observed in the FUDS driving cycle when the battery capacity was double; while only a 10% cost reduction occurred in the Highway driving cycle.

State machine control algorithm for comparison methodology

The proposed methodology of dynamically efficient energy management system is compared against a state machine control algorithm. The latter is proposed and tested by Panik [45]. Different states are formulated depending on the demanded power and vehicle speed.

1. **State 1: Motoring** ($P_L > 0, v > 0, P_L > P_{FCmin}$) If the demanded load is positive and greater than the minimum power that can be supplied by the FC, then the FC system is turned on

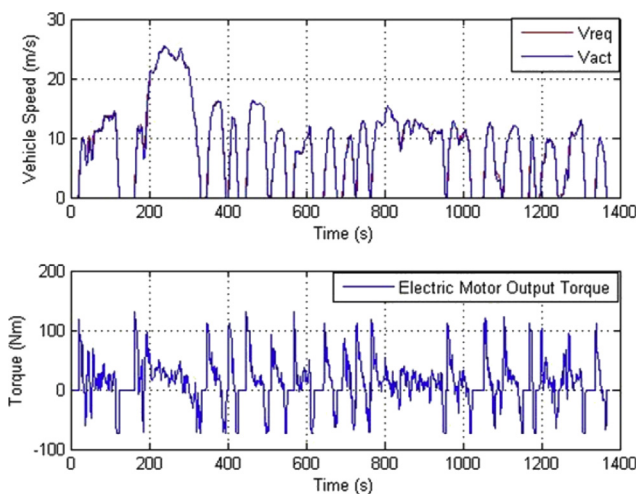


Fig. 20 – Speed and torque curve for FUDS driving cycle.

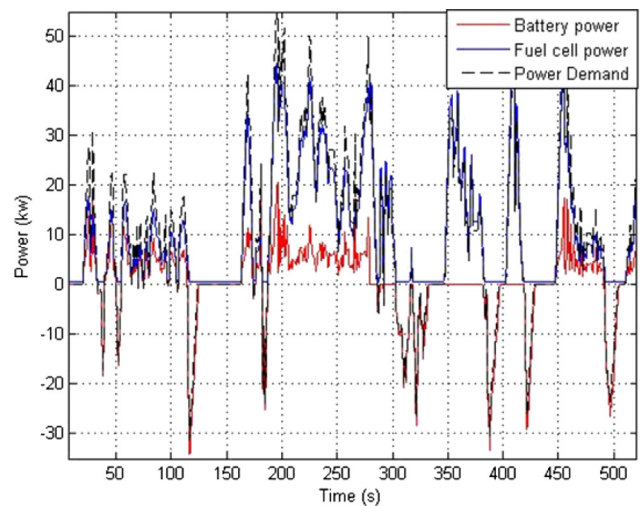


Fig. 22 – Episode of the power sources for FUDS driving cycle.

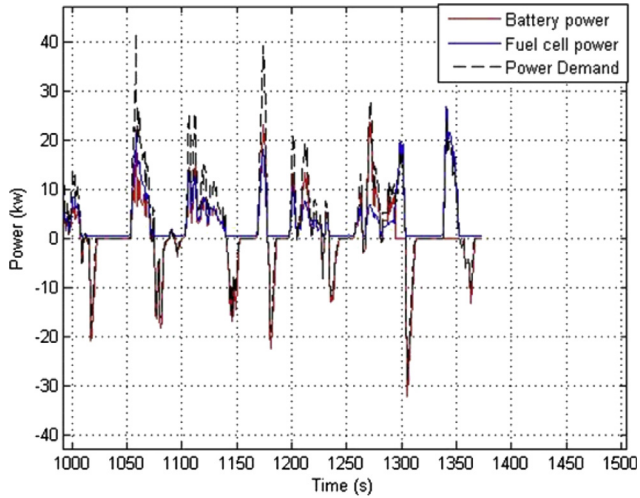


Fig. 23 – Episode of the power sources for FUDS driving cycle.

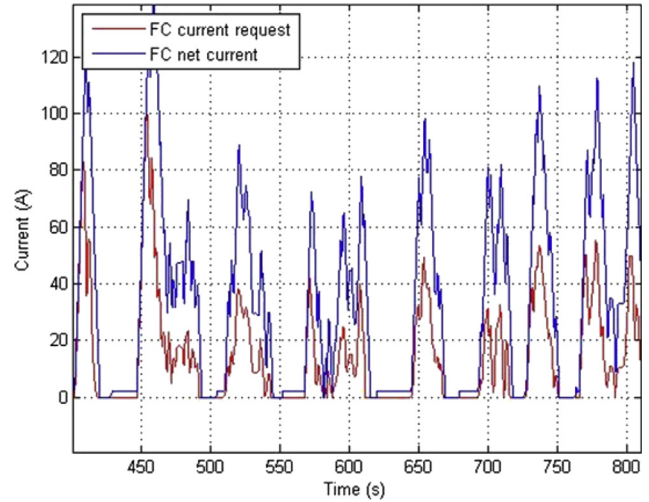


Fig. 25 – Episode of fuel cell currents for FUDS driving cycle.

and limited to the minimum power values. The battery system supplies the difference between the required load and minimum power value of the FC.

2. **State 2: Motoring** ($P_L > 0, v > 0, P_{FC-min} < P_L < P_{FCmax}$) If the demanded load is positive and ranges between the minimum and maximum power that can be supplied by the FC, then the FC system is turned on and limited to the demanded power values while preserving the ramp rate constraint. The battery system supplies the difference between the required load and supplied power value of the FC.
3. **State 3: Motoring** ($P_L > 0, v > 0, P_L > P_{FCmax}$) If the demanded load is positive and is greater than the maximum power that can be supplied by the FC, then the FC system is turned on and limited to its maximum power value while preserving the ramp rate constraint. The battery system supplies the difference between the required load and supplied power value of the FC.

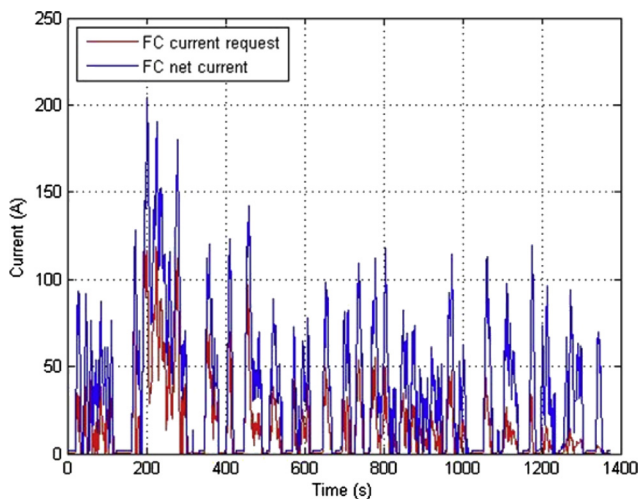


Fig. 24 – Fuel cell currents for FUDS driving cycle.

4. **State 4: Generating** ($P_L < 0, v > 0, P_L > P_{m-min}$) If the demanded load is generative and is greater than the minimum power that can be endured by the motor, then the FC system is turned on and limited to its minimum power values. The battery system supplies the difference between the required load and supplied power value of the FC.
5. **State 5: Generating** ($P_L < 0, v > 0, P_L < P_{m-min}$) If the demanded load is generative and is less than the minimum power that can be endured by the motor, then the FC system is turned on and limited to its minimum power values. The battery system supplies the difference between the minimum motor power and the supplied power value of the FC.
6. **State 6: Idling** ($P_L = 0, v = 0, P_L < P_{FCmin}$) If the demanded load is in idle mode and is less than the minimum power that can be supplied by the FC system, then the FC system is turned on and limited to its minimum power values. The battery system supplies the difference between the auxiliary power demand and the supplied power value of the FC.

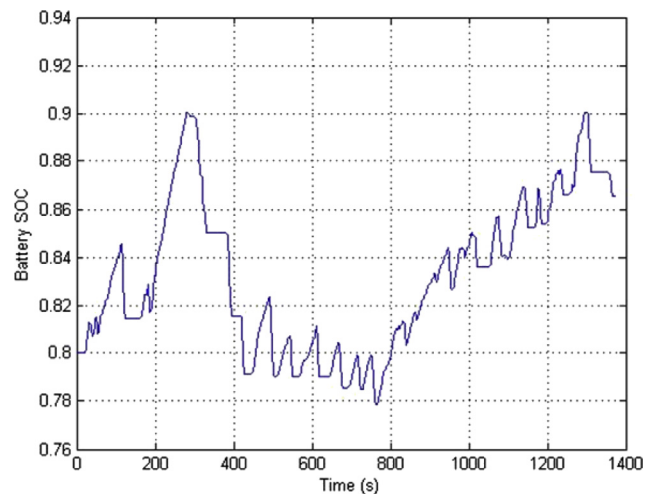


Fig. 26 – SOC for FUDS driving cycle.

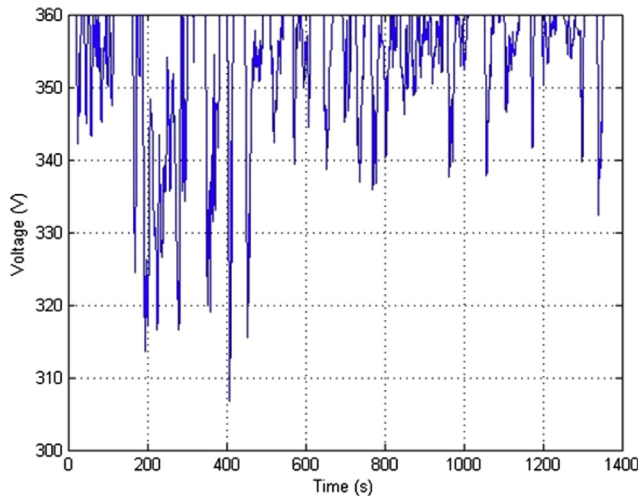


Fig. 27 – DC bus voltage for FUDS driving cycle.

Table 8 – LP results for FUDS driving cycle.

Electric energy demand (kWh)	2.3
Electric energy supplied by FC (kWh)	1.9
Electric energy supplied by BT (kWh)	0.4
Electric energy dissipated through brake (kWh)	0
Final state of charge of BT	0.5
Cost of operation (\$)	2.2

7. **State 6: Idling** ($P_L = 0$, $v = 0$, $P_L > P_{FCmin}$) If the demanded load is in idle mode and is greater than the minimum power that can be supplied by the FC system, then the FC system is turned on and limited to its minimum power value while preserving the ramp rate constraint. The battery system supplies the difference between the auxiliary power demand and the supplied power value of the FC.

The comparative study shown in Table 10 indicates that for a highway cycle, 10% improvement in cost and 5% in hydrogen consumption can be achieved. While in FUDS, up to 30% improvement can be achieved. This is the difference between an optimization method that can take all the cycle into consideration and those that have instance optimization. Improvement in urban cycle is witnessed more due to the frequent stopping which employs the battery more and saves energy from regenerative braking.

Table 9 – Doubling battery size.

	Highway driving cycle		FUDS driving cycle	
	1.9 kWh BT	3.8 kWh BT	1.9 kWh BT	3.8 kWh BT
Electric energy demand (kWh)	4.23	4.33	2.3	2.31
Electric energy supplied by FC (kWh)	3.97	3.53	1.9	1.42
Electric energy supplied by BT (kWh)	0.36	0.81	0.4	0.89
Electric energy dissipated through brake (kWh)	0.004	0.004	0	0
Final state of charge of BT	0.6	0.54	0.5	0.5
Cost of operation (\$)	4.6	4.1	2.2	1.68

Table 10 – Comparison between LP and RB EMS.

Driving cycle	H ₂ consumed (g)		Trip cost (\$)	
	LP	RB	LP	RB
FUDS	94	131	2.2	3.4
Highway	170	180	4.6	5.1

Conclusion

This paper presented a methodology to optimize the controller of FCHV based on linear programming and PID controllers. The problem formulation which takes into account the life-cycle cost of the system components considered minimizing hydrogen usage along with operational cost. Detailed Simulink model of the vehicle subsystems is built. Test simulations were performed on two driving cycles. The objective was to develop a conceptual approach for an energy optimization approach which is able to consider a wide range of constraints and targets. The simulations in this article serve to explain and to prove the process. Comparison against a state control based EMS indicates that the system cost can be reduced by 30%–10% depending on the driving cycle. Moreover, up to 30% reduction in hydrogen fuel consumption is noted. Future work will evaluate the trade-off between the battery capacity, fuel cell size, hydrogen tank volume and convenience.

Acknowledgments

The authors would like to acknowledge the support provided both by the American University of Beirut and the University of Applied Sciences for conducting this research.

REFERENCES

- [1] Ksiazek PF, Ordonez M. Swinging bus technique for ripple current elimination in fuel cell power conversion. *IEEE Trans Power Electron* 2014;29:170–8.
- [2] Zhao D, Gao F, Bouquain D, Dou M, Miraoui A. Sliding-mode control of an ultrahigh-speed centrifugal compressor for the air management of fuel-cell systems for automotive applications. *IEEE Trans Veh Technol* 2014;63:51–61.

- [3] Zheng Y, Zhao YD, Yan X, Meng K, Jun HZ, Jing Q. Electric vehicle battery charging/swap stations in distribution systems: comparison study and optimal planning. *IEEE Trans Power Syst* 2014;29:221–9.
- [4] Ju F, Li J, Xiao G, Huang N, Biller S. A quality flow model in battery manufacturing systems for electric vehicles. *IEEE Trans Automation Sci Eng* 2014;11:230–44.
- [5] Whitaker B, Barkley A, Cole Z, Passmore B, Martin D, McNutt TR, et al. A high-density, high-efficiency, isolated on-board vehicle battery charger utilizing silicon carbide power devices. *IEEE Trans Power Electron* 2014;29:2606–17.
- [6] Vural B, Boynuegri AR, Nakir I, Erdinc O, Balikci A, Uzunoglu M, et al. Fuel cell and ultra-capacitor hybridization: a prototype test bench based analysis of different energy management strategies for vehicular applications. *Int J Hydrogen Energy* 2010;35:11161–71.
- [7] Pahlevaninezhad M, Hamza D, Jain PK. An improved layout strategy for common-mode EMI Suppression applicable to high-frequency planar transformers in high-power DC/DC converters used for electric vehicles. *IEEE Trans Power Electron* 2014;29:1211–28.
- [8] Amjadi Z, Williamson SS. Digital control of a bidirectional DC/DC switched capacitor converter for hybrid electric vehicle Energy storage system applications. *IEEE Trans Smart Grid* 2014;5:158–66.
- [9] Pan X, Rathore AK. Novel bidirectional snubberless naturally commutated soft-switching current-fed full-bridge isolated DC/DC converter for fuel cell vehicles. *IEEE Trans Industrial Electron* 2014;61:2307–15.
- [10] Dalvi A, Guay M. Control and real-time optimization of an automotive hybrid fuel cell power system. *Control Eng Pract* 2009;17:924–38.
- [11] Ryu J, Park Y, Sunwoo M. Electric powertrain modeling of a fuel cell hybrid electric vehicle and development of a power distribution algorithm based on driving mode recognition. *J Power Sources* 2010;17:5735–48.
- [12] Ning Q, Xuan D, Kim Y. Modeling and control strategy development for fuel cell electric vehicles. *Int J Automot Technol* 2010;11:229–38.
- [13] Bayindir K, Gözükküçük M, Teke A. A comprehensive overview of hybrid electric vehicle: powertrain configurations, powertrain control techniques and electronic control units. *Energy Convers Manag* 2011;52:1305–13.
- [14] Pisu P, Koprubasi K, Rizzoni G. Energy management and drivability control problems for hybrid electric vehicles. In: 44th IEEE conference on decision and control, 2005 and 2005 European control conference. CDC-ECC '05; 2005. p. 1824–30.
- [15] Erdinc O, Uzunoglu M. Recent trends in PEM fuel cell-powered hybrid systems: investigation of application areas, design architectures and energy management approaches. *Renew Sustain Energy Rev* 2010;14:2874–84.
- [16] Motapon SN, Dessaint LA, Al-Haddad K. A comparative study of Energy management schemes for a fuel-cell hybrid emergency power system of more-electric aircraft. *IEEE Trans Industrial Electron* 2014;61:1320–34.
- [17] Kim MJ, Peng H. Power management and design optimization of fuel cell/battery hybrid vehicles. *J. Power Sources* 2007;165:819–32.
- [18] Ravey A, Blunier B, Miraoui A. Control strategies for fuel-cell-based hybrid electric vehicles: from offline to online and experimental results. *IEEE Trans Veh Technol* 2012;61:2452–7.
- [19] Tate E, Boyd S. Finding ultimate limits of performance for hybrid electric vehicles. SAE technical paper. 2000.
- [20] Brahma A, Guezennec Y, Rizzoni G. Optimal energy management in series hybrid electric vehicles. In: Proceedings of the 2000 American control conference, 1; 2000. p. 60–4.
- [21] Gielniak M, Shen Z. Power management strategy based on game theory for fuel cell hybrid electric vehicles. In: IEEE 60th conference in vehicular technology, 6; 2004. p. 4422–6.
- [22] Piccolo A, Ippolito L, Galdi V, Vaccaro A. Optimization of energy flow management in hybrid electric vehicles via genetic algorithms. In: Proceedings of IEEE/ASME international conference on advanced intelligent mechatronics; 2001.
- [23] Saroğlu L, Klein O, Schröder H, Küçükay F. Energy management for fuel-cell hybrid vehicles based on specific fuel consumption due to load shifting. *IEEE Trans Intelligent Transp Syst* 2012;99:1–10.
- [24] Delprat S, Lauber J, Guerra T, Rimaux J. Control of a parallel hybrid powertrain: optimal control. *IEEE Trans Veh Technol* 2004;53:872–88.
- [25] Geng B, Mills JK, Dong S. Two-stage Energy management control of fuel cell plug-in hybrid electric vehicles considering fuel cell longevity. *IEEE Trans Veh Technol* 2012;61:498–508.
- [26] Lee H, Sul AK. Fuzzy-logic-based torque control strategy for parallel-type hybrid electric vehicle. *IEEE Trans Industrial Electron* 1998;45:625–32.
- [27] Moreno J, Ortuzar ME, Dixon JW. Energy-management system for a hybrid electric vehicle, using ultracapacitors and neural networks. *IEEE Trans Industrial Electron* 2006;53:614–23.
- [28] Li CY, Liu GP. Optimal fuzzy power control and management of fuel cell/battery hybrid vehicles. *J. Power Sources* 2009;192:525–33.
- [29] Greenwell W, Vahidi A. Predictive control of voltage and current in a fuel cell 2013; ultracapacitor hybrid. *IEEE Trans Industrial Electron* 2010;57:1954–63.
- [30] Torreglosa JP, Garcia P, Fernandez LM, Jurado F. Predictive control for the energy management of a fuel-cell battery supercapacitor tramway. *IEEE Trans Industrial Informatics* 2014;10:276–85.
- [31] Lin WS, Zheng CH. Energy management of a fuel cell/ultracapacitor hybrid power system using an adaptive optimal-control method. *J Power Sources* 2011;196:3280–9.
- [32] Sadegh N, Khan B, Meisel J. Optimization of the fuel consumption of a parallel hybrid electric vehicle. In: 2005 IEEE/ASME international conference on advanced intelligent mechatronics; 2005. p. 128–33.
- [33] Gao J, Sun F, He H, Zhu GG, Strangas EG. A comparative study of supervisory control strategies for a series hybrid electric vehicle. In: Power and energy engineering conference; 2009. p. 1–7.
- [34] Pisu P, Rizzoni G. A comparative study of supervisory control strategies for hybrid electric vehicles. *IEEE Trans Control Syst Technol* 2007;15:506–18.
- [35] Garcia P, Fernandez LM, Garcia CA, Jurado F. Energy management system of fuel-cell-battery hybrid tramway. *IEEE Trans Industrial Electron* 2010;57:4013–23.
- [36] Jin K, Xinbo R, Mengxiong Y, Min X. A hybrid fuel cell power system. *IEEE Trans Industrial Electron* 2009;56:1212–22.
- [37] Phillips AM, Jankovic M, Bailey KE. Vehicle system controller design for a hybrid electric vehicle. In: Proceedings of the 2000 IEEE international conference on control applications; 2000. p. 297–302.
- [38] Fernandez LM, Garcia P, Garcia CA, Jurado F. Hybrid electric system based on fuel cell and battery and integrating a single dc/dc converter for a tramway. *Energy Convers Manag* 2011;52:2183–92.
- [39] Dinnawi R, Fares D, Chedid R, Karaki S, Jabr R. Optimized Energy management system for fuel cell hybrid vehicles. In: IEEE MELECON 2013 conference; 2014.
- [40] Kohler H. Our commitment to commercialization of fuel cell vehicles and hydrogen infrastructure. In: Fuel cells and hydrogen, joint technology initiative, 3rd stakeholders general assembly; 2010.

- [41] Guzzella L, Sciarretta A. *Vehicle propulsion systems*. 2nd ed. Springer; 2007.
- [42] Distributed energy resource guide. The California Energy Commission; 2012. <http://www.energy.ca.gov>. 2013.
- [43] Annual energy outlook. 2012. DOE/EIA-0383, [http://www.eia.gov/forecasts/aeo/pdf/0383\(2012\)](http://www.eia.gov/forecasts/aeo/pdf/0383(2012)http://www.eia.gov/forecasts/aeo/pdf/0383(2012))[http://www.eia.gov/forecasts/aeo/pdf/0383\(2012\)](http://www.eia.gov/forecasts/aeo/pdf/0383(2012)http://www.eia.gov/forecasts/aeo/pdf/0383(2012)).
- [44] Battery and energy technologies. Electropaedia; 2014. <http://www.mpoweruk.com/traction.htm>.
- [45] Panik F. *Simulation studies concerning a fuel cell hybrid bus*. SAE Technical Paper 2009-36-0402. 2009.